Mon. Not. R. Astron. Soc. **000**, 000–000 (0000) Printed 20 August 2010 (MN LATEX style file v2.2)

Morphology of the supercluster-void network in ΛCDM cosmology

Sergei F.Shandarin[1,3], Jatush V.Sheth[2,4] and Varun Sahni[2,5]
[1] *Department of Physics and Astronomy, University of Kansas,KS 66045, USA*
[2] *Inter University Centre for Astronomy & Astrophysics, Pune, India*
[3] *sergei@ku.edu*
[4] *jvs@iucaa.ernet.in*
[5] *varun@iucaa.ernet.in*

20 August 2010

ABSTRACT
We report here the *first* systematic study of the supercluster-void network in the ΛCDM concordance cosmology in which voids and superclusters are treated on an equal footing. Superclusters are defined as individual members of an over-dense excursion set and voids are defined as individual members of a complementary under-dense excursion set at the same density threshold. We determine the geometric, topological and morphological properties of the cosmic web at a large set of density levels by computing Minkowski functionals for every supercluster and void using SURFGEN (Sheth et al. 2003). The properties of the largest (percolating) supercluster and the complementary void are found to be very different from properties of individual superclusters and voids. Individual superclusters totally occupy no more than about 5% of the total volume and contain no more than 20% of mass if the largest supercluster is excluded. Likewise, individual voids totally occupy no more than 14% of volume and contain no more than 4% of mass if the largest void is excluded. Although superclusters are more massive and voids are more voluminous the difference in maximum volumes is not greater than by an order of magnitude. The genus value of individual superclusters can be ~ 5 while the genus of individual voids can reach ~ 40, implying significant amount of substructure in superclusters and especially in voids. One of our main results is that large voids, as defined through the density field (read dark matter distribution) can be distinctly non-spherical.

Key words: methods: numerical – galaxies: statistics – cosmology: theory – large-scale structure of Universe

1 INTRODUCTION

One of the great observational discoveries of recent times is the realization that we live on a cosmic web which is embedded in an accelerating Universe. Although an accelerating universe was originally established using high redshift type Ia supernovae (Knop et al. 2003; Tonry et al. 2003), the case for a 'dark energy' dominated universe has received independent support from observations of the cosmic microwave background (Spergel et al. 2003) combined with studies of galaxy clustering in the two degree field (2dF) galaxy redshift survey (Efstathiou et al. 2002). Although the nature of dark energy is still an open issue, a cosmological constant appears to agree very well with all current observations which indicate $\Omega_\Lambda \simeq 0.73$, $\Omega_m \simeq 0.23$ and $\Omega_b \simeq 0.04$ (for reviews of dark energy see Sahni & Starobinsky (2000); Sahni (2002)). Fully three dimensional large scale galaxy catalogues reveal that the cosmic web consists of an interpenetrating network of superclusters and voids. It therefore becomes important to understand and quantify the geometrical and topological properties of large scale structure in a ΛCDM cosmology in a deep and integrated manner.

The main aim of the present study is to study the supercluster-void network in ΛCDM cosmology with emphasis on the sizes, shapes and topologies of individual superclusters and voids. We shall also study the percolation properties of the full excursion set sampling the entire density field and quantify our results in terms of Minkowski functionals (hereafter, MFs). A study such as the present one will help us in comparing theory against observations. It will also help us to distinguish the salient features of ΛCDM cosmology from sister cosmologies in which dark energy is a function of time. (These issues will be discussed in detail in companion papers.)

It may be appropriate to mention that this is the first

comprehensive analysis of large scale structure geometry and morphology in which over-dense (superclusters) and under-dense (voids) regions are treated on a completely equal footing. Earlier studies have emphasized either over-densities (clusters, superclusters) or under-densities (voids) as a result of which the methods used for the analysis of these two complementary entities (superclusters/voids) often vary greatly in the literature. Thus over-dense regions have been studied using correlation functions, minimal spanning trees, shape functions etc., whereas voids have been constructed from point processes using elaborate boundary and volume filling techniques (see *e.g.* Sahni & Coles (1995); Martinez & Saar (2001) and references therein). Although the above methods do provide us with some insights into supercluster-void morphology, we shall follow an alternative route in this paper and study the properties of the supercluster-void network using the density field as our main starting point and fundamental physical quantity. The reason for this is two fold, firstly, density fields can be easily constructed from point data sets using, for example, cloud in cell (CIC) techniques (this is true both for data from N-body simulations, which we examine in this paper, as well as for galaxy distributions in three dimensions). Secondly, an elaborate surface modeling scheme, SURFGEN (short for 'surface generator'), allows us to determine the geometry, morphology and topology of excursion sets defined on a density field in a very comprehensive manner (Sheth et al. 2003). Applying SURFGEN to the density distribution in the ΛCDM model allows us to develop deep insights into the distribution of large scale structure in this model, which can be quantified using MFs and Shapefinders. Working with the density field also permits us to determine the morphological properties of the *full excursion set* describing the supercluster-void network. More detailed information is then gleaned at one particular threshold (usually associated with percolation) at which shapes and sizes of individual superclusters and voids yield rich information about properties of the cosmic web to which we belong.

Concretely, we study the large scale structure of the universe by considering the geometry and topology of isodensity surfaces $\delta(\mathbf{x}) \equiv \delta\rho(\mathbf{x})/\bar{\rho} = const$. At a given threshold $\delta_{\rm TH}$ regions having higher than threshold density ($\delta > \delta_{\rm TH}$) will be called "superclusters", while regions with $\delta < \delta_{\rm TH}$ will be called "voids". Thus, we define superclusters and voids as over-dense and under-dense connected regions bounded by one (or several) surfaces of constant density. This definition broadly corresponds to other definitions of superclusters and voids used in the literature but differs in details. Apart from obvious differences with superclusters and voids of galaxies in redshift space our approach specifies neither a particular density threshold nor the shapes of the structures. Despite these differences we call the objects of our study superclusters and voids mostly because they are nonlinear structures having sizes, volumes and masses roughly corresponding to superclusters and voids of galaxies.

We study superclusters and voids at a large number of density thresholds and construct the isodensity surfaces at every threshold to best accuracy. In contrast to many studies (see *e.g.* Blumenthal et al. (1992); Goldberg & Vogeley (2003)), we do not 'cook up' voids or superclusters with predefined shapes but isolate individual objects from the dark matter density field obtained in the N-body simulations by building the isodensity surfaces. Apart from uniformly smoothing the density field with a Gaussian filter, we do not introduce any factors that may affect the shapes or substructure in superclusters and voids of the cosmic density field. Filtering the density field may erase some small-scale features but it certainly does not introduce any new structures. Thus, we know beforehand that the real structure can be only richer and more elaborate compared to what we study after smoothing. Filtering high frequency modes is virtually implied in every physics study. This approach can be also viewed as an application of the standard excursion set technique to non-Gaussian three-dimensional fields.

One of the goals of this work is a quantitative and objective testing of some stereotypes routinely used in cosmology. Here are a few examples: both N-body simulations and redshift surveys are characterized by filamentary and sheet-like or pancake-like structures; voids are quasi-spherical bubbles in the density and/or galaxy distributions; and expand faster than the universe as whole; voids occupy most of the volume in the universe. The first problem arises when one tries to address these issues in the absence of conventional definitions. Frequently the context of the origin and usage of a particular assertion is either obscure or forgotten. Proving that some of the above cliches cannot be true does not require elaborate N-body simulations or sophisticated analysis. For instance, voids cannot *both* occupy most of the universe and expand faster than the universe because this would require the expansion of voids in *comoving space*. But this is impossible since the comoving volume is conserved ! Therefore, the expansion of some voids must clearly be at the expense of some of the others. This is one of the trivial (but important) conclusions arising from the adhesion model (Gurbatov, Saichev & Shandarin 1989; Shandarin & Zeldovich 1989; Sahni, Sathyaprakash & Shandarin 1994). At the same time it is not necessary for the interior of the squeezed voids to shrink. The interior of the void may continue to expand faster than the Hubble flow but the void eventually vanishes because its boundaries move *inwards* (Sahni, Sathyaprakash & Shandarin 1994, 1995a,b). So as the void collapses it is likely to become increasingly non-spherical. Thus, a single expanding void model while being reasonable for a crude estimate of substructure growth may be completely misleading for estimating the sizes of a realistic ensemble of voids.

Pancakes or sheet–like structures remain an unsolved controversy since their theoretical prediction by Zel'dovich in 1970. On the one hand there were numerous assertions that they had been detected in the N-body simulations or redshift surveys most of which were based on visual impressions. On the other, many believe that pancakes are not clearly seen in any realistic N-body simulations and have not been detected objectively. It is worth noting that the simulation of the structure in the hot dark matter model did not show the existence of pancakes (Klypin & Shandarin 1983) which was interpreted as the result of weak singularities corresponding to pancakes compared to considerably stronger singularities corresponding to filaments (Arnol'd, Shandarin & Zel'dovich 1982). The coarse graining unavoidable in N-body simulations erases pancakes while filaments survive. This argument has been essentially repeated by Bond, Kofman & Pogosyan (1996)

and elaborated for the probabilistic interpretation of the large-scale structure. In this study of the ΛCDM model we do not see pancakes either.

The large–scale structure in the dark matter density field is certainly different from the one observed in galaxy redshift surveys. Galaxies are at best pointwise tracers of the parent continuous dark matter density field. It is likely that they are biased tracers, and that they do not display real physical structures but structures which are strongly distorted by the mapping into redshift space. Thus, the observed superclusters and voids are not physical but only apparent objects as the retarded motion of some planets is only apparent but not real motion. At present there are only two methods of investigating real large–scale objects: by reconstructing the real space density field from peculiar velocities of galaxies and by investigating the density fields in the models that are consistent with observations such as ΛCDM.

We consider this study of the dark matter density field in real space as a first step in a systematic study of the morphology of large-scale structure. It will be followed by studies of mock and real galaxy catalogues. Understanding the morphology of the dark matter distribution in real space is an important component in understanding the physical processes determining the formation of galaxies and their motions as well as for building theoretical models of superclusters and voids.

Due to the fairly large smoothing scale adopted here, the over-density in superclusters ranges from $\delta \sim 1$ to $\delta \sim 10$, which makes them more extended ($\gtrsim$ few Mpc) and considerably less dense than galaxy clusters in (for instance) the Abell catalogue.

The rest of the paper is organized as follows. In Section 2 we briefly describe the density fields used in this study. In Section 3 we define and very briefly discuss the morphological measures which we apply to study the cosmic web. Sec. 4 provides the relation of the filling factors used in this study with the probability density function. Sec. 5 discusses the morphological properties of individual superclusters and voids. Sec. 6 describes substructure in superclusters and voids. A discussion of some properties of Minkowski functionals is contained in Sec. 7. Section 8 summarizes our main results.

2 DARK MATTER DISTRIBUTION IN VIRGO SIMULATIONS

We use dark matter distributions in a flat model with $\Omega_0 = 0.3$, $\Omega_\Lambda = 0.7$, $h = 0.7$ (ΛCDM). The initial spectrum was taken in the form suggested by Efstathiou, Bond & White (1992) with the shape parameter $\Gamma = 0.21$.

The amplitude ($\sigma_8 = 0.9$) of the power spectrum in the model is set so as to reproduce the observed abundance of rich galaxy clusters at the present epoch. A detailed discussion of the cosmological parameters and simulations can be found in Jenkins et al. (1998).

The density fields generated by the VIRGO simulations have been studied in several papers (see e.g. Springel et al. (1998); Scoccimarro, Couchman & Frieman (1999)); this is the first systematic study of global and local morphology when both over-dense and under-dense regions are measured by the same method.

SURFGEN operates on three-dimensional pixelized maps. Therefore we first generate the density field from the distribution of dark matter particles. This process was described in detail in Sheth et al. (2003); here we present a brief summary. The data consist of 256^3 particles in a box of size 239.5 h^{-1}Mpc. We fit a 128^3 grid to the box. Thus, the size of each cell is 1.875 h^{-1}Mpc. Here we follow the smoothing technique used by Springel et al. (1998) which they adopted for their preliminary topological analysis of the Virgo simulations. In the first, we apply a Cloud in Cell (CIC) technique to construct a density field on the grid. Next we smooth this field with a Gaussian kernel which offers us an extra smoothing length-scale. We study the field smoothed with $L_s = 5$ h^{-1}Mpc but also present the global MFs for the field smoothed with 10 h^{-1}Mpc for comparison. The scale of $L_s = 5$ h^{-1}Mpc is a fiducial smoothing scale in many studies of both density fields in N-body simulations and galaxy fields from redshift surveys; see for example, Grogin & Geller (2000). The Gaussian kernel for smoothing that we adopt here is

$$W(r) = \frac{1}{(\pi)^{\frac{3}{2}} L_s^3} exp\left(-\frac{r^2}{L_s^2}\right). \quad (1)$$

Since the kernel is isotropic, it is likely to diminish the true extent of anisotropy in filaments and pancakes. This effect could be minimized by considering anisotropic kernels and/or smoothing techniques based on the wavelet transform. An even more ambitious approach is to reconstruct density fields using Delaunay tesselations using a technique reported by van de Weygaert (2002). Density fields reconstructed in this manner appear to preserve anisotropic features and may therefore have some advantage over conventional 'cloud-in-cell' techniques followed by an isotropic smoothing (Schaap & Weygaert 2000). Thus, as far as one of the goals is to utilize the geometry of the patterns to discriminate between the models, such smoothing schemes should prove more powerful. We hope to return to these issues in further publications.

We scan the density fields at 99 values of the density threshold, all equispaced in the filling factor FF_C defined as

$$FF_{\rm C}(\delta_{\rm TH}) = \frac{1}{V_{tot}} \int \Theta(\delta - \delta_{\rm TH}) d^3x, \quad (2)$$

where $\Theta(x)$ is the Heaviside Theta function and $\delta = (\rho - \bar{\rho})/\bar{\rho}$ is the density contrast. The supercluster filling factor $FF_{\rm C}$ measures the volume-fraction in regions which satisfy the 'supercluster' criterion $\delta_{\rm sc} \geqslant \delta_{\rm TH}$. In the following, we use $FF_{\rm C}$ along with the void filling factor $FF_{\rm V} \equiv 1 - FF_{\rm C}$ as a parameter to label the density contours. The relation between $FF_{\rm C}$ and density contrast threshold can be seen in Fig. 1.

At each level of the density field (labeled by $FF_{\rm C}$ or $FF_{\rm V}$), we construct a catalogue of superclusters (over-dense regions) and voids (under-dense regions) based on a grid realization of the Friends of Friends (FOF) algorithm.

Next we (i) run the SURFGEN code on each of these superclusters/voids to model surfaces for each of them and (ii) determine the Minkowski Functionals (MFs) for all superclusters/voids at the given threshold (these are referred to in the literature as partial MFs). Global MFs are partial

MFs summed over all superclusters. Thus, at each level of the density, we first compute the partial MFs and then the global MFs.

3 MORPHOLOGICAL PARAMETERS

Since the 1970s, theory, N-body simulations, and, most importantly, galaxy redshift surveys have strongly suggested that the components of the large-scale structure can be roughly placed in three classes: compact quasi-spherical or slightly elliptical structures like Abell clusters, long filaments like the famous 'bridge' connecting the Coma cluster and A1367, (Gregory & Thompson (1978)) and voids. There have also been claims that pancake-like concentrations of galaxies have been observed Fairall (1998); Martinez & Saar (2001). The voids have often been claimed to have quasi-spherical or slightly elliptical shapes. Most of these claims have been based on visual impressions. In particular, statistics used in studies of voids often assumed that voids are spherical or close to spherical thereby precluding any other possibility.

In this work we study the geometry and topology of the regions bounded by the isodensity surfaces and therefore make no prior assumptions about the shapes of superclusters and voids. It is worth noting that some regions may have more than one boundary surface and possess nontrivial topology of the boundaries. The complete characterization of an arbitrarily complex region in three dimensions obviously cannot be achieved if only a few numbers are used. At best one can try to design some basic characteristics that serve a particular purpose. Our purpose is to provide basic measures suitable for quantification of typical components of the large-scale structure: superclusters and voids.

Four Minkowski functionals are effective non-parametric descriptors of the morphological properties of surfaces in three dimensions (Mecke, Buchert & Wagner 1994; Matsubara 2003; Sheth et al. 2003). They are

- *Volume* V enclosed by the surface, S,
- *Area* A of the surface,
- *Integrated mean curvature* C of the surface,

$$C = \frac{1}{2}\oint_S \left(\frac{1}{R_1}+\frac{1}{R_2}\right) da, \tag{3}$$

where R_1 and R_2 are the principal radii of curvature at a given point on the surface.

- *the Euler characteristic*

$$\chi = \frac{1}{2\pi}\oint_S \left(\frac{1}{R_1 R_2}\right) da. \tag{4}$$

Although for our purpose the Euler characteristic is a more convenient quantity than genus, G (see Appendix for a discussion) the latter has been used more often in cosmology. The genus is uniquely related to the Euler characteristic $G = 1 - \chi/2$ and thus carries exactly the same information. We measure the above parameters for every region in both over-dense and under-dense excursion sets at 99 density thresholds equispaced in the filling factor from $FF = 0.01$ to $FF = 0.99$.

As demonstrated in Sahni, Sathyaprakash & Shandarin (1998); Sathyaprakash, Sahni & Shandarin (1998) particular ratios of Minkowski functionals called "Shapefinders" provide us with a set of non-parametric measures of sizes and shapes of objects. Therefore, in addition to determining MFs we shall also derive the Shapefinders, T (Thickness), B (Breadth) and L (Length) defined as follows:

$$T = \frac{3V}{A}, \quad B = \frac{A}{C}, \quad L = \frac{C}{4\pi}. \tag{5}$$

The three Shapefinders describing an individual region bounded by one or several isolated surfaces of constant density have dimensions of length and provide us with an estimate of the regions 'extension': T is the shortest and thus describes the characteristic thickness of the region or object, L is typically the longest and characterizes the length of the object; B is intermediate and can be associated with the breadth of the object. This simple interpretation is obviously relevant only for fairly simple shapes. The choice of the coefficients in eq. 5 results in a sphere having all three sizes equal to its radius $T = B = L = R$. A triaxial ellipsoid has values of T, B and L close but not equal to the lengths of its three principal semi-axes: shortest, intermediate and the longest respectively. It is worth noting that T, B and L are only the estimates of three basic sizes (semi-axes) of an object which work quite well on such objects as a triaxial ellipsoid and torus (Sahni, Sathyaprakash & Shandarin 1998; Sathyaprakash, Sahni & Shandarin 1998; Sheth et al. 2003) but no three numbers can describe an arbitrary, complex three-dimensional shape.

An indicator of 'shape' is provided by a pair of dimensionless Shapefinder statistics

$$P = \frac{B-T}{B+T}; \quad F = \frac{L-B}{L+B}, \tag{6}$$

where P and F are measures of Planarity and Filamentarity respectively ($P, F \leqslant 1$). A sphere has $P = F = 0$, an ideal filament has $P = 0, F = 1$ while $P = 1, F = 0$ for an ideal pancake. Other interesting shapes include 'ribbons' for which $P \sim F \sim 1$. When combined with the genus measure, the triplet $\{P, F, G\}$ provides an example of *shape-space* which incorporates information about topology as well as morphology of superclusters and voids.[1]

4 PERCOLATION AND GLOBAL TOPOLOGY

4.1 Filling factors and one-point function

A characteristic of the density field which is both simple and useful is the one-point probability density function, $p(\delta)$, where $\delta \equiv (\rho - \bar{\rho})/\bar{\rho}$. In this study we use the integral

$$FF_C(\delta) = P(\delta) = \int_\delta^\infty p(\delta')d\delta' \tag{7}$$

known as the cumulative probability function (cpf) as a major quantity parameterizing the excursion sets. It measures the fraction of volume in the excursion set, $\delta > \delta_{\rm TH}$. In order to compare supercluster and void parameters we also use the under-density filling factor

[1] Non-geometrical shape-statistics based on mass moments etc. can give misleading results when applied to large scale structure, as demonstrated in Sathyaprakash, Sahni & Shandarin (1998).

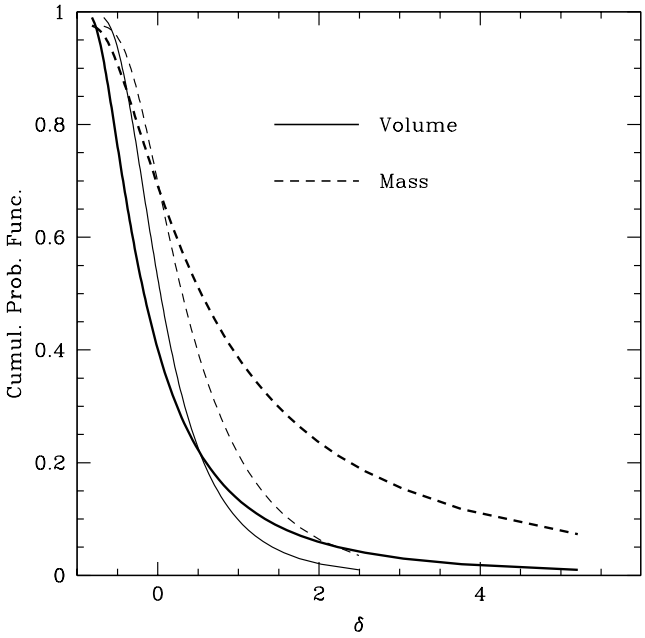

Figure 1. Cumulative probability functions of the density contrast in the Virgo simulations of the ΛCDM model smoothed with L_s=5 $h^{-1}$and 10 h^{-1}Mpc are shown by the thick and thin solid lines respectively. The fractions of mass in the excursion sets are shown by the dashed line. The cumulative probability function equals the filling factor FF_C.

$$FF_V(\delta) = 1 - FF_C(\delta) = \int_{-1}^{\delta} p(\delta')d\delta'. \quad (8)$$

The filling factor $FF_C = FF_C(\delta)$ is shown in Fig. 1 (thick solid line) for ΛCDM smoothed on the length scale of L_s=5 h^{-1}Mpc. In addition, the thick dashed line shows the fraction of mass in the excursion set for the same smoothing scale. From Fig. 1 we find that the density field is 'nonlinear' ($\delta > 1$) in a relatively small fraction ($\lesssim$ 15%) of the total volume. However, the difference between these two curves is the first clear demonstration of nonlinearity of the density field. Convergence to the Gaussian distribution with the growth of the smoothing scale is demonstrated by the two thin lines corresponding to the smoothing scale of L_s=10 h^{-1}Mpc.

4.2 Percolation

Understanding percolation is essential for understanding the morphology of the supercluster-void network. Percolation is important because the properties of superclusters and voids radically change at the percolation transitions (see Fig. 2). The left panel shows: (i) the fractional volumes in the largest supercluster and void (dashed lines) and (ii) the total volume in all superclusters and voids after the largest object has been removed from the sample (solid lines). The right panel shows mass fractions in all four components. At relatively high thresholds $\delta_C \gtrsim 1.8$ corresponding to small filling factors $FF_C \lesssim 0.07$ the largest supercluster has insignificant volume and mass compared to the total volume or mass

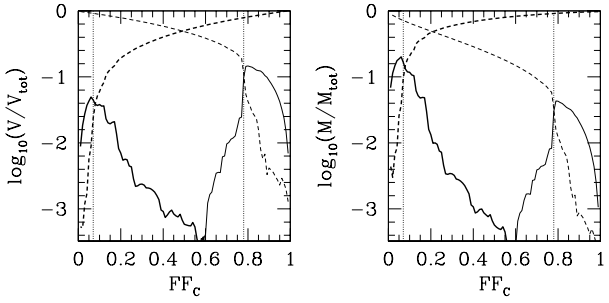

Figure 2. Left panel: the fractions of the total volume occupied by the largest supercluster (thick dashed line), all superclusters but the largest one (thick solid line), largest void (thin dashed line), and all voids but the largest one (thin solid line) are shown for the density field in the ΛCDM model smoothed with L_s=5 h^{-1}Mpc as a function of the filling factor, FF_C. Right panel: the y-axis shows the fraction of mass in the components shown in the left panel. Vertical dotted lines show the percolation threshold for superclusters ($FF_C \approx 0.07$) and voids ($FF_C \approx 0.78$; note: $FF_V = 1 - FF_C \approx 0.22$).

contained in the over-dense excursion set, $\delta > \delta_{\rm TH}$. During the percolation transition at $FF_C \approx 0.07$ corresponding to $\delta_C \approx 1.8$, both volume and mass in the largest supercluster rapidly grow, overtaking the volume and mass in the entire excursion set, and completely dominating the entire sample from this point onwards. The largest void behaves in a qualitatively similar manner if plotted versus FF_V. At $FF_V \lesssim 0.22$, $\delta_V \lesssim -0.5$ its volume is small compared to the volume of the under-dense excursion set, $\delta < \delta_{\rm TH}$, but at the percolation transition $FF_V \approx 0.22$, $\delta_V \approx -0.5$, it takes over and from then on remains the dominant structure in the under-dense excursion set. Since $FF_C \equiv 1 - FF_V$ the void percolation transition takes place at $FF_C \approx 0.78$ as shown in Fig. 2.

Two obvious conclusions can be drawn from the above discussion. First, at percolation the object having the largest volume becomes very different from all remaining objects, therefore it must be studied separately. Second, individual objects – both superclusters and voids – must be studied in the corresponding phase *before percolation occurs* in the corresponding phase. Both superclusters and voids reach their largest sizes, volumes and masses just before percolation sets in.

Figure 2 also shows that at $FF_C > 0.5$ superclusters dominate by volume while at $FF_C < 0.5$ voids dominate. In the range $0.2 \lesssim FF_C \lesssim 0.7$ corresponding to $1.6 \gtrsim \delta \gtrsim -0.43$, no more than 10% of volume is occupied by non-percolating objects, while the remaining more than 90% of entire volume is occupied by just two largest objects: percolating supercluster and the percolating void. In the range between the two percolation thresholds $FF_C \approx 0.07$ and $FF_C \approx 0.78$, both largest objects percolate and therefore the density field has a sponge like structure. The interval of sponge like structure in a Gaussian field is between $FF_C \approx 0.16$ and $FF_C \approx 0.84$. Therefore nonlinear gravitational evolution has shifted it toward smaller FF_C and increased its range by a little bit from 0.68 (=0.84−0.16) to 0.71 (=0.78−0.07).

It is worth stressing that the shift and length of the sponge like interval are determined by the percolation

thresholds which in general are two independent parameters. As a result of these shifts the interval of the so called "meat-ball" topology (when no supercluster percolates) has reduced compared to the Gaussian case from $FF_C \approx 0.16$ to $FF_C \approx 0.07$ and the interval of the "bubble" topology (when no void percolates) is increased from $FF_V \approx 0.16$ to $FF_V \approx 0.22$. All the numbers obviously depend on the adopted smoothing scale but the sign and type of change must be universal for the ΛCDM model.

For both superclusters and voids $FF = FF_{\rm max} + FF_{\rm ind}$, where $FF_{\rm ind}$ stands for the fractional volume occupied by all objects excluding the largest one, and $FF_{\rm max}$ is the fractional volume in the largest object. Further since, $FF_{\rm max}/FF_{\rm ind} \gg 1$ in the the most part of the range between two percolation thresholds for both superclusters and voids, it is not surprising that $FF^C_{\rm max} = FF^V_{\rm max}$ almost exactly at $FF_C = FF_V = 0.5$. A similar result was found in the models with power law initial spectra (Yess & Shandarin 1996).

Percolation is characterized by many features, the most conspicuous being the rapid merger of disjoint parts of the excursion set into one connected structure spanning the entire volume. Merging of superclusters occurs when the density threshold is reduced whereas merging of voids correspond to the growth of the threshold. Spanning of the largest supercluster or void throughout the whole volume results in connection of the opposite faces of the cubic volume by this structure which explains the term *percolation*. Although in principle the percolation transition can be determined by checking if the opposite faces of the cube are connected, in practice it is more robust to identify percolation using other properties of the excursion set (Klypin 1987; Klypin & Shandarin 1993). As the estimators of the percolation threshold we use the following four ratios

$$m^{(i)} = \frac{MF^{(i)}_{\rm max}}{MF^{(i)}_{ES}}, \quad i = 1, 2, 3, 4, \tag{9}$$

where $MF^{(i)}$ is one of four quantities: volume, area, integrated mean curvature, or mass ($MF^{(1)} = V$, $MF^{(2)} = A$, $MF^{(3)} = C$, $MF^{(4)} = M$). The subscript "max" is self-explanatory, and "ES" stands for the entire excursion set. At percolation these ratios grow extremely rapidly from very small values to unity. The maximum rate of growth $\delta m^{(i)}/\delta(FF)$ can be used as a reliable estimator of the percolation threshold as shown in Fig. 3. All four parameters detect the percolation transitions at $FF_C \approx 0.07$ for superclusters and at $FF_V \approx 0.22$ for voids. These transitions correspond to the density contrast $\delta_C \approx 1.8$ for superclusters and $\delta_V \approx -0.5$ for voids.

Figure 4 compares the largest supercluster with the largest void. Three Minkowski functionals and the fraction of the mass in the largest objects are shown as a function of the corresponding filling factor. The difference of two curves in every panel is a significant indication of non-Gaussianity of the density field. All Gaussian curves must coincide in every panel and show maximum growth at $FF^{SC}_C = FF^V_V \approx 0.16$. The nonlinear gravitational evolution in the ΛCDM model shifts the percolation transition in the over-dense excursion set toward smaller filling factors ($FF_C : \ 0.16 \rightarrow 0.07$) and in the under-dense excursion set toward larger filling factors ($FF_V : \ 0.16 \rightarrow 0.22$). Again

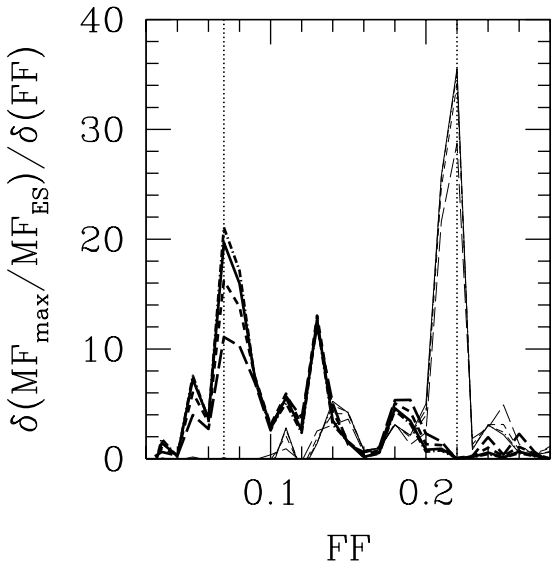

Figure 3. Estimates of the percolation thresholds. The rate of growth $\delta m^{(i)}/\delta(FF)$ for the four estimators listed in eq. 9 is shown as a function of FF. Thick lines show results for superclusters. All four curves consistently peak at $FF = FF_C = 0.07$. Thin lines show similar quantities for voids with a distinct peak at $FF = FF_V = 0.22$. Solid, short dashed, long dashed, and dot-dashed lines show the volume, area, curvature, and mass estimators respectively. Vertical dotted lines mark the percolation thresholds.

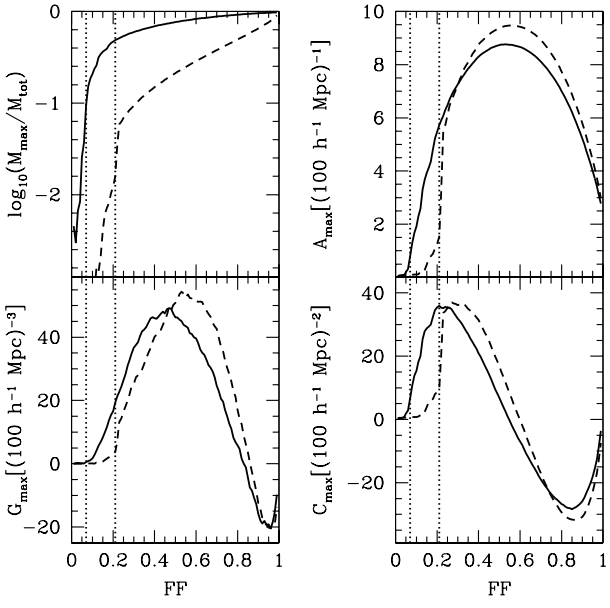

Figure 4. The mass fraction and Minkowski functionals of the largest (by volume) supercluster and void in the ΛCDM model smoothed with the L_s=5 h^{-1} Mpc window as a function of corresponding filling factor ($FF = FF_C$ for the largest supercluster; $FF = FF_V$ for the largest void). Solid and dashed lines show the parameters of the largest supercluster and void respectively. Vertical dotted lines mark the percolation transitions.

the particular numbers depend on the choice of the smoothing scale but the sign of the effects is independent of the smoothing scale. At smaller smoothing scales as well as for any adaptive smoothing having a better resolution in high density regions the supercluster percolation threshold must decrease ($FF_C < 0.07$) and void percolation threshold must increase ($FF_V > 0.22$). On the other hand, increasing the smoothing scale would result in a continuous reduction of differences between superclusters and voids and their ultimate convergence to Gaussian curves in every panel (not shown).

It is worth noting that the percolation transition in voids is more conspicuous than that in superclusters. The transition is particularly clearly marked by $A_{\max}$ and $C_{\max}$ curves. All curves look differently after percolation as well. However, in order to precisely evaluate the significance level of these differences one needs to analyze more than one realization and/or have larger simulation volume.

4.3 Global topology

It is interesting to compare the percolation and genus statistics. Both were suggested as tests for assessing the connectedness of the large-scale structure. In a series of papers Zel'dovich and Shandarin (Zeldovich 1982; Shandarin 1983; Shandarin & Zeldovich 1983) raised the question of topology of large-scale structure and suggested percolation statistic as a discriminator between models. The percolation test was first applied to a redshift catalog (compiled by J. Huchra) by Zeldovich, Einasto & Shandarin (1982) and then Einasto et al. (1984) who found that the connectivity between galaxies in this catalog was significantly stronger than for a Poisson distribution. In contrast, a non-dynamical computer model having approximately correct correlation functions up to the fourth order (Soneira & Peebles 1978) showed significantly weaker connectivity than observed. Thus, percolation was able to detect connectedness in the galaxy distribution. It was also demonstrated that three lowest order correlation functions (two-, three- and four-point functions) are not sufficient to detect the connectedness in the galaxy distribution.

A few years later Gott, Melott & Dickinson (1986) (see also Melott (1990) for a review) suggested the genus statistic as a discriminator between various models of large-scale structure. Although both percolation and genus statistics characterize density fields and are sensitive to the connectedness of the large scale structure, each carries significantly different information. It is important to remember that the genus refers to a surface which is the *interface* between over-dense and under-dense regions (defined at a given density threshold). An interpretation of genus as a characteristic of a three dimensional object (supercluster or void) bounded by this surface is not unique and certainly non-trivial if the region has a complicated shape. For instance, both a full sphere and a doughnut with a bubble in its body have genus of 0.

Figure 5 shows the genus curve in a slightly unusual form (see also Sahni, Sathyaprakash & Shandarin (1997)). The half of the curve corresponding to high density thresholds is shown as a function of the over-density filling factor FF_C (solid line) while the other half corresponding to low thresholds is plotted as a function of the under-density filling factor FF_V (dashed line). This allows to better illustrate the deformations of the curve due to nonlinear effects. The Gaussian genus curve is symmetric for positive and negative thresholds thus both parts of it overlap in Fig. 5 (dotted line). The vertical dashed lines mark three thresholds: the supercluster percolation threshold at $FF = FF_C \approx 0.07$, the void percolation threshold at $FF = FF_V \approx 0.22$ and the both percolation thresholds in a Gaussian field at $FF = FF_C = FF_V \approx 0.16$.

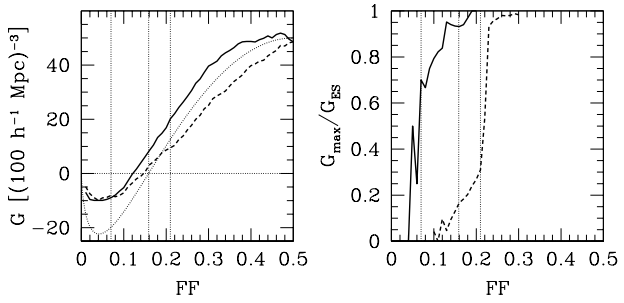

Figure 5. *Left panel*: the global genus is shown as a function of the filling factor for the density field smoothed with $L_s = 5\ h^{-1}$ Mpc. The half of the curve corresponding to high density thresholds is plotted as a function of FF_C (solid line) while the other half corresponding to low density thresholds is plotted as a function of FF_V (dashed line). For comparison, the dotted line shows the Gaussian genus curve having the same amplitude. The vertical dotted lines mark two percolation thresholds in the ΛCDM ($FF = FF_C \approx 0.07$ and $FF = FF_V \approx 0.22$) and Gaussian field ($FF = FF_C = FF_V \approx 0.16$). *Right panel*: the percolation transitions in the same density field as indicated; the genus of the largest supercluster (solid line) and largest void (dashed line). The vertical dotted lines mark the percolation thresholds similar to left panel.

A marked decrease in the amplitude of the genus curve compared to the Gaussian curve at small FF is noticeable for both over-dense and under-dense excursion sets. (Small $FF \equiv$ high density for superclusters and low density for voids.) The global genus curve has no significant features at either percolation threshold $FF_C \approx 0.07$ or $FF_V \approx 0.22$. The right panel of Fig. 5 shows the ratios of the genus of the largest object G_{max} to the global genus of the excursion set G_{ES} for both superclusters (solid line) and voids (dashed line). Both percolation curves shown in the right panel would overlap in the case of a Gaussian field (not shown) and demonstrate the percolation transition at $FF \approx 0.16$. The other indicators of the percolation transitions (Eq. 9) are in excellent agreement with the right panel of Fig. 5 which can be seen by comparing Fig. 5 with Figs. 3 and 4. The splitting of the percolation curves shown in Fig. 5 (right panel) as well as in Fig. 4 clearly demonstrates non-Gaussianity of the density field.

After percolation takes place the genus of the largest object considerably increases (Fig. 6) which manifests its complex shape. The length and therefore filamentarity of the largest object radically changes after percolation takes place (see Fig. 6 and 7) and cannot be easily interpreted. On the other hand, the breadth and thickness, (and consequently also the planarity), grow much more gradually with the growth of the corresponding filling factor and in this sense are similar to non-percolating objects. The *mean*

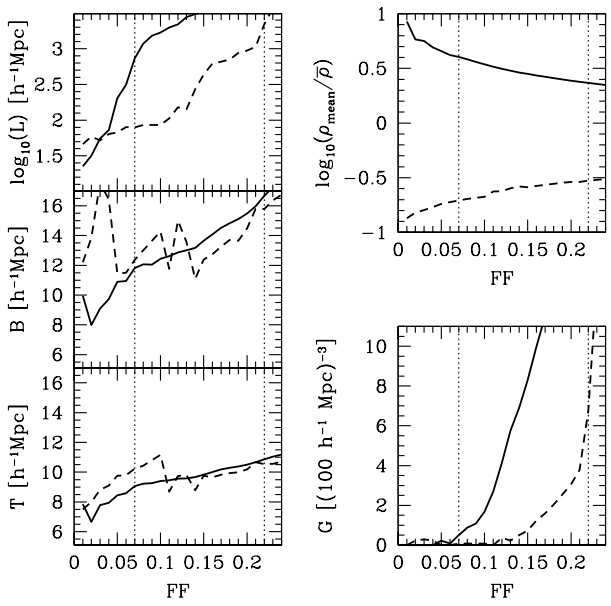

Figure 6. The length, breadth, thickness, mean density, and genus of the largest (by volume) supercluster (solid lines) and void (dashed line) in the ΛCDM model smoothed with $L_s = 5\,h^{-1}$ Mpc are shown as a function of of FF_C and FF_V respectively. Vertical dotted lines show the supercluster ($FF = FF_C \approx 0.07$) and void ($FF = FF_V \approx 0.22$) percolation thresholds.

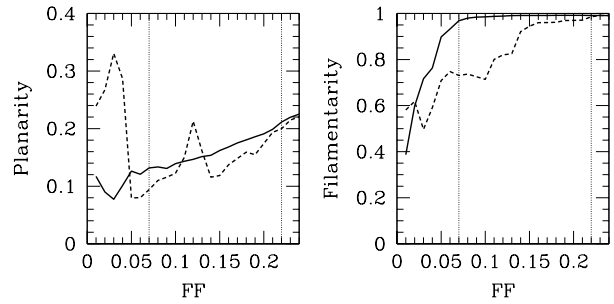

Figure 7. Planarity and filamentarity of the largest structures as a function of the filling factor. The largest supercluster and void are shown by solid and dashed lines respectively. Vertical dotted lines show the supercluster ($FF = FF_C \approx 0.07$) and void ($FF = FF_V \approx 0.22$) percolation thresholds.

density of the percolating supercluster at the percolation transition is $\bar{\rho}_{\rm SC} \approx 4\bar{\rho}$ so that $\delta_{\rm SC} \approx 3$. The corresponding value for the percolating void is $\bar{\rho}_{\rm V} \approx 0.3$ and $\delta_{\rm V} \approx -0.7$. Both $\delta_{\rm SC}$ and $\delta_{\rm V}$ are significantly different from the percolation threshold for superclusters ($\delta_{\rm C} = 1.8\bar{\rho}$) and voids ($\delta_{\rm V} = -0.5$) respectively (see Figure 6).

5 INDIVIDUAL SUPERCLUSTERS AND VOIDS

In this section we carry out comparative statistical analysis of physical and geometrical parameters of superclusters and voids. We stress that the largest supercluster and the largest void both are excluded from this analysis. Before percolation transition they both are extreme outliers and after percolation they have nothing in common with the other objects. The total number of individual objects is shown in Fig. 8. There are numerous small objects among both superclusters and voids which dominate by numbers at every threshold (right panel of Fig. 8). Including them into the statistical analysis along with large objects would seriously affect all the parameters. One way to deal with this problem would be the computation of weighted parameters, *i.e.* by mass for superclusters and by volume for voids. This actually corresponds to computing one or a few moments of the probability distribution function which also may be misleading because the distribution functions are strongly non-Gaussian. We analyze only the the most massive superclusters making 90% of all mass in non-percolating over-dense objects and most voluminous voids making 90% of total volume in non-percolating under-dense objects. The smallest over-dense and under-dense objects are excluded from the analysis. Figure 8 shows the number density in (100 h^{-1} Mpc)$^{-3}$ units for both large (left panel) and small (right panel) objects. Despite the smallest objects make only 10% of mass or volume they are more numerous then the largest objects making the most of mass or volume.

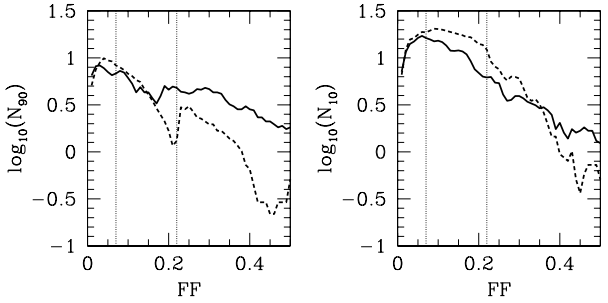

Figure 8. *Left panel*: the number density (in (100 h^{-1} Mpc)$^{-3}$ units) of the most massive superclusters making 90% of all *mass* contained in non-percolating superclusters as a function of the filling factor FF_C is shown by solid line. The number density of the largest voids making 90% of all *volume* contained in non-percolating voids as a function of the filling factor FF_V is shown by dashed line. *Right panel*: the number density of the least massive superclusters making 10% of all *mass* contained in non-percolating superclusters as a function of the filling factor FF_C is shown by solid line. The number density of the smallest voids making 10% of all *volume* contained in non-percolating voids as a function of the filling factor FF_V is shown by dashed line. Two vertical dotted lines mark percolation thresholds for superclusters ($FF_C \approx 0.07$) and voids($FF_V \approx 0.22$)

5.1 Masses, volumes and mean densities

We begin with the analysis of masses, volumes and mean densities

$$\rho_{mean} \equiv \frac{M}{V} \tag{10}$$

which are probably the most important factors among those that determine the visual impression. They are also the least ambiguous.

Figure 9 shows the masses, volumes and mean densities of superclusters (left) and voids (right) at various thresholds parameterized by the corresponding filling factor. The

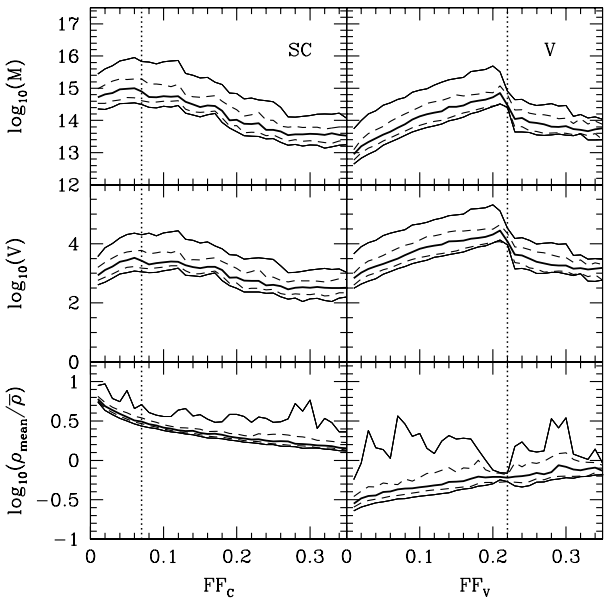

Figure 9. Mass (in solar masses), volume (in (h^{-1} Mpc)^3), and mean density (*i.e.* $\rho_{mean} = (M/V)/\bar{\rho}$) of all but the largest structure are shown as a function of the volume filling factor FF_C. Thick solid line is the median of the distribution, dashed lines mark 25-75% interval, and thin solid lines show the third largest and third smallest value in the distribution. Vertical dotted lines show the percolation thresholds in over-dense and under-dense excursion sets. The supercluster and void parameters are shown in the right and left panels respectively.

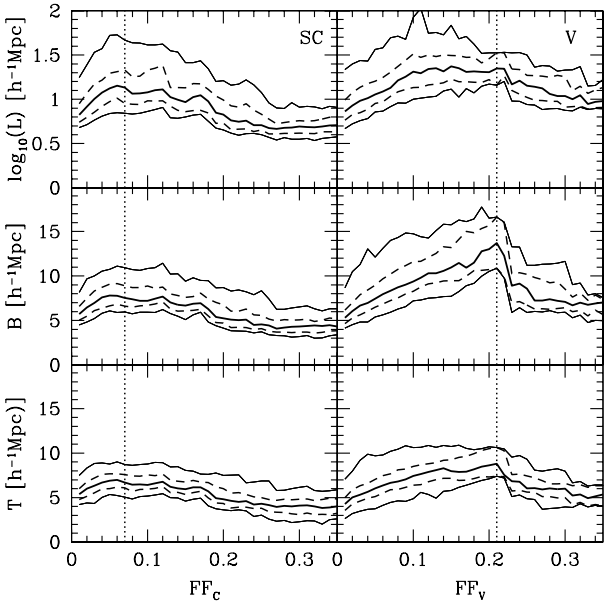

Figure 10. The length L, breadth B, and thickness T of all but the largest object is shown as a function of the corresponding filling factor. The notations are as in Fig. 9.

thick solid lines show the median of the distribution, the dashed lines show the 50% interval (25% largest and 25% smallest are beyond this interval), and thin solid lines show the 95% interval. The intervals are highly asymmetric with respect to the median which indicates the non-Gaussianity of all distribution functions. Every distribution function has a long tail at large values. Both superclusters and voids have largest masses and volumes around the corresponding percolation threshold although the maximum is more distinct in the case of voids. As one might anticipate, voids are less massive and more voluminous than superclusters. However, the difference is not huge at the chosen smoothing scale. The median mass reaches a maximum about 10^{15} $M_\odot$ for superclusters and $10^{14.8}$ $M_\odot$ for voids. The median volume in the corresponding maximum is about 3×10^3 $(h^{-1}Mpc)^3$ for superclusters and about 3×10^4 $(h^{-1}Mpc)^3$ for voids. The mean densities of the superclusters are well above the mean density before percolation and gradually decrease after percolation takes place however remaining above the mean density in the universe. As expected the mean density of voids increases with the growth of FF_V corresponding to the growth of the density threshold. It is somewhat surprising that the volumes of superclusters do not change much with the threshold, the masses change more but not greater than by an order of magnitude.

5.2 Sizes and Shapes

Three characteristic sizes and shapes of superclusters and voids can be estimated from Minkowski functionals of every object (eq. 5 and 6). Figure 10 shows the median and 50% and 95% intervals for the length, breadth and thickness of the superclusters and voids. The sizes of superclusters are shown as a function of FF_C, while the sizes of voids as a function of FF_V. It is surprising that the median thickness of superclusters depends on the threshold so weakly; it is within 4−6 h^{-1}Mpc interval for a range of thresholds between $0 \lesssim \delta \lesssim 6$. This may indicate that the actual thickness of superclusters is significantly smaller and the measured values reflect the width of the smoothing window. The breadth of superclusters is not much larger than the thickness and it is likely that this quantity is also affected by the width of the filtering window. Voids are a little fatter than superclusters and their median thickness reaches about 9 h^{-1} Mpc at the percolation threshold. Interestingly voids are also wider and longer than superclusters (please note the logarithmic scale used for length). Recalling that the size parameters are normalized to the radius of the sphere rather than to diameter we conclude that the longest 25% of superclusters are longer than about 50 h^{-1} Mpc and 25% of voids are longer than about 60 h^{-1} Mpc.

The shape parameters of superclusters and voids are shown in Fig. 11. The median planarities of superclusters are small which means that in the ΛCDM universe the dark matter density field smoothed with $5h^{-1}$Mpc typically has no pancake-like superclusters with the diameters greater than about 10 h^{-1} Mpc. The outliers can reach planarity $P \approx 0.3$ corresponding to the ratio $B/T \approx 1.4$ which is not large either. In addition, it happens only at quite large filling factors where the density threshold is quite low and only very few superclusters are left (see Fig. 8). Voids show an opposite

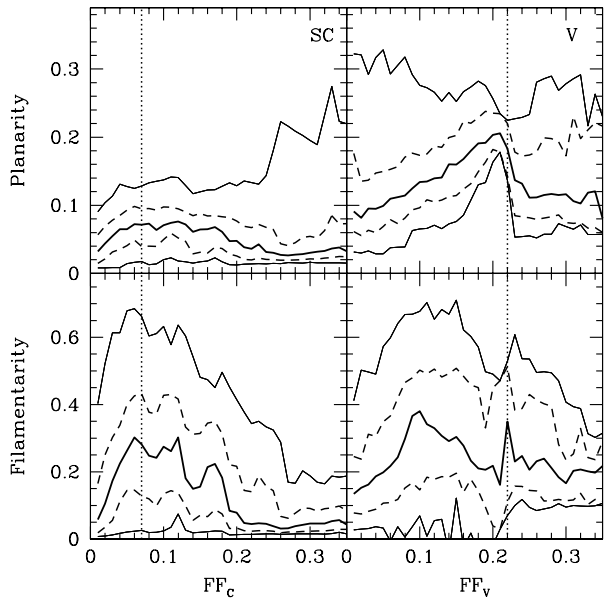

Figure 11. The planarity, P and filamentarity, F of all but the largest object is shown as a function of the corresponding filling factor. The notations are as in Fig. 9.

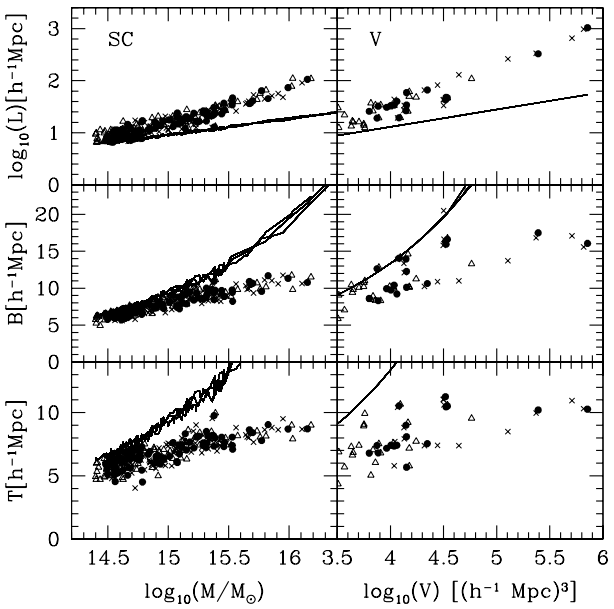

Figure 12. The length, breadth, and thickness versus mass for superclusters and versus volume for voids at percolation. Solid circles show the relation at percolation thresholds: $FF_C = 0.07$ for superclusters and $FF_V = 0.22$ for voids. Crosses show the parameters before percolation ($FF_C = 0.06$ for superclusters and $FF_V = 0.21$ for voids) and empty triangles after percolation ($FF_C = 0.08$ for superclusters and $FF_V = 0.23$ for voids). Solid lines show the radius of the sphere having the same volume as the corresponding object. Note the logarithmic scale used for the length. Three lines correspond to three different thresholds.

trend to superclusters: voids are significantly more planar than superclusters and the largest planarities in voids occur at small filling factors. Filamentarities are significantly higher for both over-dense and under-dense objects: median values peak at about 0.35 ($L/B \approx 2$). The outliers could be considerably more elongated $F > 0.7$ (*i.e.* $L/B > 6$). As we shall see in the next section, the more massive a supercluster or more voluminous a void, the greater is its tendency to be filamentary.

5.3 Correlations between morphological and physical parameters

Both superclusters and voids reach their largest sizes near their respective percolation thresholds: $FF_C \approx 0.07$ for superclusters and $FF_V \approx 0.22$ for voids. Figure 12 shows the scatter plots of three characteristic sizes (L, B, and T) versus mass for superclusters and versus volume for voids. The combined plots are made for $FF_C = 0.06$, 0.07 and 0.08 for superclusters and for $FF_V = 0.21$, 0.22 and 0.23 for voids. The solid lines show the radius of a sphere having the same volume as a given object ($R = (3V/4\pi)^{1/3}$). All three sizes show a significant correlation with the mass: the greater the mass the greater the thickness, breadth and length. The thickness and breadth approximately double their values and length grows over an order of magnitude when mass increases from about $10^{14.5}$ $M_\odot$ to $10^{16.5}$ $M_\odot$. Both the thickness and breadth are considerably smaller than the radius R of a sphere having similar volume for large superclusters ($M \gtrsim 10^{15}$ $M_\odot$) as well as for large voids ($V \gtrsim 10^4$ $(h^{-1}\,Mpc)^3$). On the other hand the length is considerably greater than R. This is another manifestation of anisotropies of the large-scale objects.

The corresponding plots of planarities and filamentarities show a similar correlation: the larger the mass of a

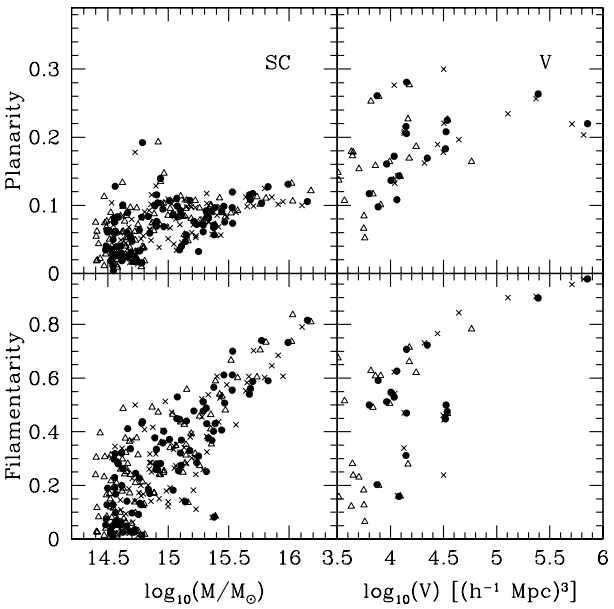

Figure 13. The planarity and filamentarity vs mass (for superclusters) and vs volume (for voids) at percolation. Notations are as in Fig 12.

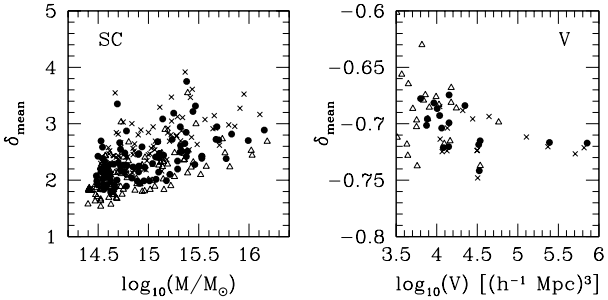

Figure 14. *Right panel*: correlation of the mean density contrast ($\delta_{mean} = M/(\bar{\rho}V) - 1$) of a supercluster with its mass at percolation. *Left panel*: correlation of the mean density contrast of a void with its volume at percolation. Notations are as in Fig 12.

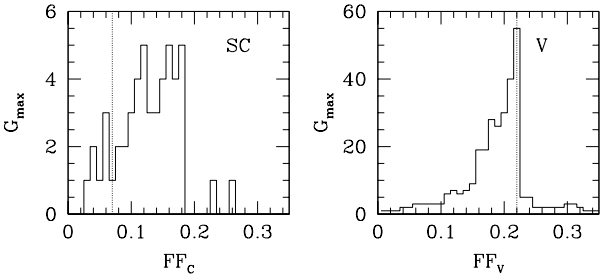

Figure 15. The maximum of genus as a function of the filling factor. Left panel: the maximum genus in isolated superclusters. Right panel: the maximum genus in isolated voids. Note the difference of the scales on the vertical axis.

supercluster or the larger the volume of a void, the greater its planarity and filamentarity (Fig. 13). One can clearly see that the largest objects (superclusters with $M > 10^{15}\ M_\odot$ and voids with $V > 10^4\ (h^{-1}Mpc)^3$ are the most anisotropic large-scale objects. Note that voids display a higher level of planarity when compared to superclusters. Indeed, one of the most noticeable results of this analysis is evidence that voids defined near the onset of percolation of the underdense excursion set are *significantly* non-spherical. Finally, the larger the mass of a supercluster the greater its mean density and the more voluminous a void the lower its mean density (Fig. 14).

6 SUBSTRUCTURE IN SUPERCLUSTERS AND VOIDS

Visual inspection shows that superclusters and voids have noticeable substructure. Isolated voids inside superclusters and isolated clusters and superclusters inside voids are obvious examples. Theory (Kofman et al. 1992; Sahni, Sathyaprakash & Shandarin 1994) and targeted N-body simulations (Beacom, et al. 1991; Gottlöber et al. 2003) show that voids are also filled with smaller filaments of high density. In the ΛCDM universe these filaments are strong enough to survive smoothing on a scale $L_s = 5\ h^{-1}Mpc$. Figure 15 shows the maximum of the genus of superclusters and voids. In order to interpret it properly we need to explain how to interpret the genus of an object.

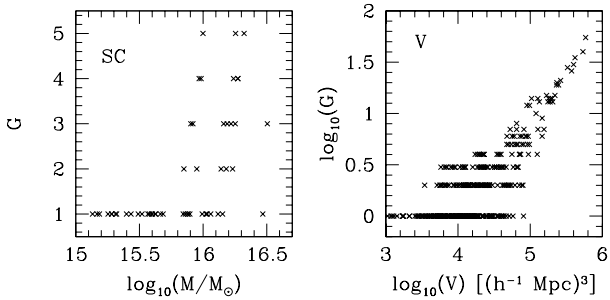

Figure 16. The genus-mass relation is shown for isolated superclusters in the left hand side panel. The genus-volume relation is shown for voids on the right. Every isolated supercluster and void having genus greater than zero at all density thresholds is shown. The mass is given in the solar units and the volume in $(h^{-1}$ Mpc$)^3$. Note the difference of the scales on the vertical axis.

A standard interpretation of genus in cosmological literature (see *e.g.* Melott (1990)) says

$$G = \text{(number of holes)-(number of isolated regions)}+1, \quad (11)$$

this requires additional clarifications. First, "holes" stand for fairly complex mathematical objects that do not always coincide with the simple minded meaning of the word. For instance, a cavity in a tooth is not a hole, a bubble in a glass of champagne is not a hole either, but a tunnel through a mountain is a hole. Second, "number of isolated regions" means the number of isolated pieces of the surface that define the boundaries of the object. For instance, a region bounded by two nested spheres (a thick spherical shell) has two disconnected pieces of the boundary surface and no tunnels, therefore its genus is -1. A torus has surface in one piece but it has a tunnel, thus its genus equals $+1$. Consider an object topologically homeomorphic to a sphere (G=0), *i.e.* only one boundary surface and no tunnels. Adding a tunnel increases the genus by one and adding a bubble inside the body reduces the genus by one. Thus, a doughnut with a bubble of air in its body has genus 0, exactly as a full sphere.

Figure 15 shows that the genus of an isolated supercluster can be as large as five. It means that there are *at least* five tunnels through the supecluster. The number of tunnels could be even greater if it also had a few smaller isolated voids inside. The vast majority of superclusters are topologically isomorphic to a sphere *i.e.* , $G = 0$, but the most massive ones have genus greater than unity. A supercluster with genus of unity is homeomorphic to a doughnut and one with genus of two to a pretzel. The substructure of voids is considerably more complex. The largest genus of voids detected in this simulation is 55, therefore at least 55 filaments span through the void !

Figure 16 shows the correlation between genus and mass (for superclusters) or volume (for voids). Largest superclusters $M \gtrsim 10^{15}\ M_\odot$ have a nontrivial topology. Generally the more massive supercluster the greater chance of complex topology. Voids display even stronger correlation between genus and volume.

7 SYMMETRY OF GLOBAL MINKOWSKI FUNCTIONALS

The global Minkowski functionals were introduced in cosmology by Mecke, Buchert & Wagner (1994) and since then have been used in many studies, see *e.g.* Schmalzing et al. (1999); Sheth et al. (2003). Since the Minkowski functionals are additive[2] we obtain them by simple summation over all objects at every density threshold. As discussed in Sheth et al. (2003)) computing the global Minkowski functionals poses some problem in the case of periodic boundary conditions. However, as shown in Appendix it can be solved if Minkowski functionals are computed for every supercluster and void at a given threshold.

In Gaussian fields three global Minkowski functionals (area A, integrated mean curvature C, and genus G) have certain symmetries as functions of the filling factor. In addition, the number of positive peaks, N_+ in the excursion set equals the number of negative troughs, N_-:

$$A(1-FF_C) = A(FF_C), \quad (12)$$

$$C(1-FF_C) = -C(FF_C), \quad (13)$$

$$G(1-FF_C) = G(FF_C), \quad (14)$$

$$N_-(1-FF_C) = N_+(FF_C). \quad (15)$$

The departure from these symmetries manifests the non-Gaussianity of the field even before a comparison with the corresponding Gaussian functions. Figure 17 shows the violation of the symmetry in the global Minkowski functionals in the ΛCDM model smoothed with L_s=5 h^{-1}Mpc and 10 h^{-1} Mpc. The half of every curve corresponding to positive thresholds ($\delta_{\rm TH} \gtrsim 0$) is plotted as a solid line and the other half as a dashed line. The curves corresponding to smaller smoothing scale have higher amplitudes and are shown by thick lines. One can see that while the curves corresponding to L_s=5 h^{-1}Mpc are likely to be non-Gaussian,they almost overlap at L_s=10 h^{-1}Mpc.

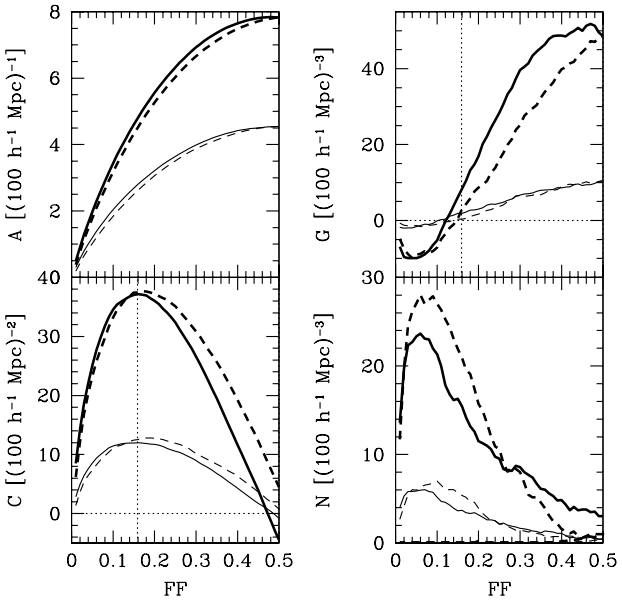

Figure 17. Symmetry test for the density field smoothed with L_s=5 h^{-1} Mpc (thick lines) and 10 h^{-1} Mpc (thin lines). Global area, curvature and genus at $FF < 0.5$ are shown as a function of $1-FF$ by dashed lines. In addition, the sign of the global curvature is also changed. The number of voids is shown by dashed line. The vertical dotted lines mark $FF = 0.16$ where the Gaussian genus curve crosses the zero level and the integrated mean curvature has a maximum.

8 SUMMARY AND DISCUSSION

We have studied the large–scale network in the dark matter density field in real space obtained from N-body simulations by VIRGO consortium (Jenkins et al. 1998). The density distribution has been smoothed with a Gaussian window ($L_s = 5\ h^{-1}\ Mpc$).

The major goal of the study was quantitative description and comparison of over-dense and under-dense regions which were dubbed as superclusters and voids respectively. We conducted the measurements of four Minkowski functionals for every individual supercluster and void selected at 99 density thresholds equispaced in terms of the filling factor (Eqs. 2, 7 and 8) with the SURFGEN code. By computing the shapefinders (Eqs. 5 and 6) from Minkowski functionals we estimated the sizes and shapes of every supercluster and void. In this study we did not assume any shape or other characteristics for the large-scale objects. Instead we have measured the morphology and various other characteristics of the objects as they were defined by the isodensity surfaces. It is worth stressing that in our study the superclusters and voids have been defined as three-dimensional regions with closed boundary surfaces[3].

The main results of our investigation are summarized below:

- Individual superclusters totally occupy no more than about 5% of the total volume and comprise no more than 20% of mass if the largest (*i.e.* percolating) supercluster is excluded (Fig. 2).
- The maximum of the total volume and mass comprised by all superclusters except the largest one is reached approximately at the percolation threshold: $\delta \approx 1.8$ corresponding to $FF_C \approx 0.07$.
- Individual voids totally occupy no more than 14% of volume and contain no more than 4% of mass if the largest void is excluded (Fig. 2).
- The maximum of the total volume and mass comprised by all voids except the largest one is reached at about the void percolation threshold: $\delta \approx -0.5$ corresponding to $FF_V \approx 0.22$.
- Between these two percolation thresholds all superclusters and voids except the largest ones take up no more than about 10% of volume and mass. Both largest supercluster and void span throughout the whole space and have a very large genus. Therefore they have no well defined sizes, volumes, masses or easily defined shapes.

[2] Note, genus is not additive but the Euler characteristic is additive.

[3] In some studies voids are viewed as the regions between filaments connected in a closed loop; for example, see Fig.4 in Sheth & Van de Weygaert (2003).

• Although superclusters are more massive and voids are more voluminous the difference in maximum volumes reached at the corresponding percolation thresholds is not much greater than an order of magnitude (see Fig. 9). The difference in maximum masses is even smaller than the difference in volumes.

• The volumes, masses and geometrical sizes of superclusters increase as the density threshold decreases and reach maximum values at about the percolation threshold ($\delta \approx 1.8$). At lower thresholds all parameters decrease as the threshold continues to decrease.

• The sizes of voids are significantly larger than those of superclusters even in the density field smoothed with $L_s = 5\ h^{-1}\ Mpc$.

• The length of a quarter of the most massive superclusters exceeds 50 h^{-1} Mpc. The most voluminous voids are even longer: 25% of them are longer than 60 h^{-1} Mpc. The longest non-percolating supercluster is as long as 100 h^{-1} Mpc and the longest non-percolating void is as long as 200 h^{-1} Mpc. Both are comparable to the size of the box ($239.5\ h^{-1}\ Mpc$) and therefore may be affected by the boundaries.

• The genus value of individual superclusters can be ~ 5 while the genus of individual voids can reach ~ 55. This implies significant amount of substructure in superclusters and voids.

• Voids have considerably more developed substructure than superclusters. This is in a general agreement with other studies of voids (Grogin & Geller 2000; Peebles 2001).

• One of our main results is that voids, as defined through the density field (read dark matter distribution) can be distinctly non-spherical. Whether this result carries over to voids in galaxy surveys will depend upon the nature of the baryon-dark matter biasing and also on whether the density field is sampled in real or in redshift space. Since gravitational lensing probes the density field directly, our results are likely to be of some relevance both for ongoing as well as future weak lensing surveys of large scale structure.

• The planarities of both superclusters and voids are quite low $P \lesssim 0.3$. This implies that the pancake-like structures in the dark matter density in real space are not typical in the ΛCDM model. We are stressing that this conclusion may be affected by the size of the smoothing window.

• The percolation thresholds as well as some other parameters depend on the smoothing scale and for smaller smoothing scales or adaptive filtering windows the supercluster percolation threshold must decrease ($FF_C^{perc.} < 0.07$) and the void percolation threshold increase ($FF_V^{perc.} > 0.22$).

9 ACKNOWLEDGMENTS

VS and SS acknowledge support from the Indo-US collaborative project DST/NSF/US (NSF-RP087)/2001. SS acknowledges the support from the Observatory Cote d'Azur Nonlinear Cosmology Program (Nice France) in summer 2003 when most of the analysis was done. The trip to Nice was funded by AAS. JVS is supported by the Senior Research Fellowship of the Council of Scientific and Industrial Research (CSIR), India. The simulations studied in this paper were carried out by the Virgo Supercomputing Consortium using computers based at Computing Centre of the Max-Planck Society in Garching and at the Edinburgh Parallel Computing Centre. The data are publicly available at *www.mpa-garching.mpg.de/NumCos*.

REFERENCES

Arnol'd, V.I., Shandarin, S.F. & Zel'dovich, Ya.B., 1982, Geophys. Astrophys. Fluid Dynamics, 20, 111

Beacom, J., Dominik, K., Melott, A.L., Perkins, S., & Shandarin, S.F. 1991, ApJ, 372, 351

Blumenthal, G. R., da Costa, L. N., Goldwirth, D. S., Lecar, M. and Piran, T., 1992, ApJ, 388, 234

Bond, J.R., Kofman, L.A. and Pogosyan, D., 1996, Nature, 380, 603.

Efstathiou, G., Moody, S., Peacock, J. et al., 2002, MNRAS Pink Pages, 330, 29

Efstathiou, G., Bond, J.R., White, S.D.M., 1992, MNRAS, 258, 1p

Einasto, J., Klypin, A.A., Saar, E. and Shandarin, S.F., 1984, MNRAS, 206, 529

Fairall, A., 1998, *Large-Scale Structure in the Universe*, John-Wiley & Sons in association with Praxis Publishing, Chichester.

Goldberg, D.M., Vogeley, M., 2003, astro-ph/0307191

Gott, J.R., Melott, A.L. & Dickinson, M., 1986, ApJ, 306, 341

Gottlöber, S., Lokas, E.L., Klypin, A. Hoffman, Y., 2003, MNRAS, 344, 715

Gurbatov, S. N., Saichev, A. I., and Shandarin, S. F. 1989, MNRAS 236, 385.

Gregory, S.A.and Thompson, L.A., 1978, ApJ,222, 784

Grogin, N.A. and Geller, M.J., 2000, AJ, 119,32

Jenkins, A.R. et al. (for the Virgo Constortium), 1998, ApJ, 499, 20

Klypin, A.A. 1987, Soviet Astron., 31, 8

Klypin, A.A. & Shandarin, S.F., 1983, MNRAS, 204, 891

Klypin, A.A. & Shandarin, S.F., 1993, ApJ, 413, 48

Knop, R.A., et al., (2003) astro-ph/0309368

Kofman, L.A., Pogosyan, D., Shandarin, S.F. and Melott, A., 1992, ApJ, 393, 450.

Martinez, V.J. and Saar, E. "Statistics of the galaxy distribution", Chapman and Hall.

Matsubara, T., 2003, ApJ, 584, 1

Mecke, K.R., Buchert, T. & Wagner, H., 1994, A&A, 288, 697

Melott, A.L., 1990, Phys. Rep., 193, 1

Peebles, P.J.E., 2001, ApJ, 557,495.

Sahni, V., 2002, Class. Quantum Grav., 19, 3435.

Sahni, V. and Coles, P., 1995, Phys.Rept., 262, 1.

Sahni, V., Sathyaprakash, B.S. & Shandarin, S.F., 1994, ApJ **431**, 20.

Sahni, V., Sathyaprakash, B.S. & Shandarin, S.F., 1995, *"Voids and their evolution in the adhesion model"* in: *Proceedings of the International workshop on Large Scale Structure in the Universe, Potsdam, Germany*, September 18-24 1994, Eds. J.P. Mucket, S. Gottlober and V. Muller p. 147. (World Scientific Publishing).

Sahni, V., Sathyaprakash, B.S. & Shandarin, S.F., 1995, *" Voids and Adhesion theory"* in: *Proceedings of the International Workshop "Birth of the Universe and Funda-*

mental Physics" Rome, Italy, 18 - 21 May, 1994. Editor: F. Occhionero, Springer-Verlag 1995, p. 205.
Sahni, V., Sathyaprakash, B.S. & Shandarin, S.F., 1997, ApJL, 476, L1
Sahni, V., Sathyaprakash, B.S. & Shandarin, S.F., 1998, ApJL, 495, L5
Sahni, V. and Starobinsky, A.A., 2000, IJMP, D9, 373
Sathyaprakash, B.S., Sahni, V. & Shandarin, S.F., 1998, ApJ, 508, 551
Schaap, W.E. and van de Weygaert, R., 2000, A & A, 363, L29-L32
Schmalzing, J., Buchert, T., Melott, A.L., Sahni, V., Sathyaprakash, B.S. and Shandarin, S.F., 1999, ApJ, 526, 568.
Scoccimarro, R., Couchman, H.M.P., & Frieman, J., 1999, ApJ, 517,531
Sheth, R. and Van de Weygaert, R., 2003, astro-ph/0311260
Sheth, J.V., Sahni, V., Shandarin, S.F. & Sathyaprakash, B. 2003, MNRAS, 343, 22
Shandarin, S.F. 1983, Sov. Astron. Lett., 9, 104
Shandarin, S.F. & Zeldovich, Ya.B., 1983, Comments Astrophys. 10, 33
Shandarin, S.F. & Zeldovich, Ya.B., 1989, Rev. Mod. Phys.,61,185
Soneira, R.M. & Peebles, P.J.E. 1978, Astron. J., 83, 845
Spergel, D.N. et al., 2003, astro-ph/0302209
Springel, V. et al. (for the Virgo Consortium), 1998, MNRAS, 298, 1169
Tonry, J.L., et al. 2003, astro-ph/0305008
van de Weygaert, R., 2002, "Froth across the Universe, Dynamics and Stochastic Geometry of the Cosmic Foam", arXiv: astro-ph/0206427
Yess, C. and Shandarin, S.F., 1996, ApJ, 465, 2.
Zel'dovich, Ya.B. 1982, Sov. Astron. Lett., 8, 102
Zeldovich, Ya.B., Einasto, J. and Shandarin, S.F., 1982, Nature, 300, 407

10 APPENDIX: GLOBAL MINKOWSKI FUNCTIONALS IN A BOX WITH PERIODIC BOUNDARY CONDITIONS

In computing the Minkowski functionals of individual large-scale objects (superclusters or voids) we assume that the boundary surface of every object is closed however it may consist of several disconnected parts. If the region is cut by a box boundary it is always closed by the corresponding part of the box face. We also assume that the partial Minkowski functionals are measured for all superclusters and voids at the same set of density thresholds. In this case the evaluation of the global Minkowski functionals with periodic boundary conditions can be done as follows.

• *Volume*: The total volume is obviously independent of the assumption of periodicity $V^{(cp)} = V^{(c)} = \sum v_i^{(c)}$ where $v_i^{(c)}$ are the volumes of individual superclusters and $V^{(cp)}$ and $V^{(c)}$ denote the global volumes in periodic and non-periodic boxes.

• *Area*: Let us denote the total area of the superclusters at given filling factor $FF \equiv FF_c$ as $A^{(c)} = \sum a_i^{(c)}$ and the total area of voids as $A^{(v)} = \sum a_i^{(v)}$. Then, the sum of two becomes

$$A^{(c)} + A^{(v)} = 2A^{(p)} + A^{(box)} \tag{16}$$

where $A^{(p)}$ is the total area of the excursion set in the box with periodic boundary conditions and $A^{(box)}$ is the total area of the box boundary (see Fig. 18 for an illustration). For periodic boundary conditions the global area of the over-dense excursion set obviously equals the global area of the under-dense excursion set since it is the area of the common interface surface. Solving the above equation for $A^{(p)}$ one obtains

$$A^{(p)} = \frac{A^{(c)} + A^{(v)} - A^{(box)}}{2}. \tag{17}$$

• *Integrated mean curvature*: The isodensity surfaces is constructed by the triangulation described in detail in Sheth et al. (2003). It is convenient for the further calculation of the global integrated mean curvatures to split the sum into two parts: one is the sum over the inner edges and the other is the sum over the edges lying on the box boundary

$$C^{(c)} = \sum_{\text{all edges}} c_j^{(c)} = \sum_{\text{in. edges}} c_k^{(c)} + \sum_{\text{b. edges}} c_i^{(c)} \tag{18}$$

and

$$C^{(v)} = \sum_{\text{all edges}} c_j^{(v)} = \sum_{\text{in. edges}} c_k^{(v)} + \sum_{\text{b. edges}} c_i^{(v)}. \tag{19}$$

For the inner edges the contributions to global mean curvatures of the superclusters and voids have the same magnitude but opposite signs

$$c_k^{(c)} = \frac{1}{2} l_k(\pi - \varphi_k) = -c_k^{(v)}, \tag{20}$$

where φ_k is the angle between two surface triangles having common edge as shown in Fig. 18. Please note that in this equation we use the angle between the triangle planes while in eq. 6 (Sheth et al. 2003) we used the angle between the normals to the triangles. If the edge lies on the box boundary the relation is less trivial.

Consider a region R_i being cut by the box face into two pieces R_{i1} and R_{i2} as schematically shown in Fig. 18. The dashed lines show the projections of the opposite faces of the box. The plane of the figure is assumed to be orthogonal to the edge lying on the faces of the box and having the length l_i. This assumption is made only for convenience of the illustration and does not affect the calculation. We consider the input to the mean integrated curvature from the edge l_i. The code treats the regions R_{i1} and R_{i2} as two separate regions, therefore

$$c_i^{(c)} = \frac{1}{2}[l_i(\pi - \varphi_i) + l_i(\pi - \theta_i)] = \pi l_i - \frac{1}{2} l_i(\varphi_i + \theta_i). \tag{21}$$

However, if R_i was treated as one region which corresponded to the periodic boundary conditions then we would have

$$c_i^{(cp)} = \frac{1}{2}\pi l_i - \frac{1}{2} l_i(\varphi_i + \theta_i). \tag{22}$$

Thus, each edge lying on the face of the box contributes to the global integrated mean curvature extra $\frac{1}{2} l_i \pi$ compared to the periodic case. Similar reasoning yields for the adjacent void

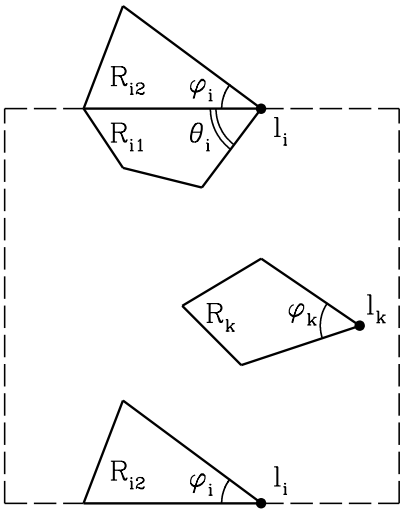

Figure 18. Two superclusters are schematically shown. One is inside the box (internal) and the other is cut into two pieces by the boundary of the box.

$$c_i^{(v)} = \frac{1}{2} l_i(\varphi_i + \theta_i) \tag{23}$$

and

$$c_i^{(vp)} = -\frac{1}{2}\pi l_i + \frac{1}{2} l_i(\varphi_i + \theta_i). \tag{24}$$

Note that $c_i^{(cp)} = -c_i^{(vp)}$ as it should be.

For the face edges we have

$$c_i^{(v)} = -c_i^{(c)} + \pi l_i \tag{25}$$

Now we have all the terms for equations 18 and 19 and after simple and straightforward calculations obtain the global mean integrated curvatures for superclusters and voids for periodic boundary conditions in terms of non-periodic quantities

$$C^{(cp)} = \frac{1}{2}(C^{(c)} - C^{(v)}) = -C^{(vp)}. \tag{26}$$

• *The Euler characteristic*: Three kinds of elements of the triangulated surface are triangle faces, edges and vertices. The Euler characteristic of the triangulated surface is

$$\chi = F - E + V, \tag{27}$$

where F, E and V are the total numbers of faces (triangles), edges and vertices respectively for both closed and open surfaces.

A related measure of topology often used in cosmology is the genus $G = 1 - \chi/2$. Although the two quantities are uniquely related and therefore carry exactly the same information the Euler characteristic has more convenient mathematical properties. As we shall see below including the surfaces with boundaries (*i.e.* open surfaces) into analysis is very useful in many cases in particular in dealing with the boundary conditions. For such surfaces the genus is fractional: *e.g.* the Euler characteristic of a patch is $\chi_p = 1$ and thus its genus is $G_p = -1/2$. As a result the standard interpretation (eq. 11) cannot be directly applied. Secondly, and more importantly, the Euler characteristic is additive while genus is not. It means that the Euler characteristic of a set of disconnected surfaces is simply the sum over all members of the set $\chi_g = \sum_i \chi_i$ but the genus is not $G_g \neq \sum_i g_i$. For example, three isolated spheres have a genus of $G_g = -2 \neq \sum g_i = 0$ while $\chi_g = \sum \chi_i = 6$. In our study we use Minkowski functionals for both the global description of the density field and individual objects. Thus, the additivity of a parameter becomes a very useful property.

Similarly to the previous discussion of the integrated mean curvature we split each number into two: one is the input from the elements lying inside the box and the other from the elements lying on the boundary *i.e.* faces of the box

$$\chi = (F_{in} - E_{in} + V_{in}) + (F_b - E_b + V_b), \tag{28}$$

where subscripts "in" and "b" correspond to the internal elements of triangulation lying inside of the box and on the boundaries of the box respectively. In the periodic case there are neither triangles nor edges or vertices on the faces of the box, therefore

$$\chi^{(p)} = F_{in} - E_{in} + V_{in} \tag{29}$$

for both superclusters and voids because it is the characteristic of the common interface surface.

The boundary group of terms gives different results for superclusters and voids. In the case of superclusters $F_b^{(c)} - E_b^{(c)} + V_b^{(c)} = \chi_b^{(c)}$ is the Euler characteristic of the "cluster boundary surface" i.e. the surface consisting of all regions on the faces of the box that have been used for closing the superclusters cut by the boundary. And in the case of voids it is obviously the remaining of the box surface which can be called the "void boundary surface" $F_b^{(v)} - E_b^{(v)} + V_b^{(v)} = \chi_b^{(v)}$. For instance, consider a simple case when there is only one cluster cut by a box face. Assuming non-periodic boundary conditions and closed boundary surfaces for all superclusters the parts of cluster surface consists of two simply connected pieces each homeomorphous to a circle and thus $\chi_b^{(c)} = 2$. The void boundary surface is homeomorphous to a sphere with two holes (not tunnels) and thus $\chi_b^{(v)} = 0$. If there were n superclusters cut by the box boundaries then $\chi_b^{(c)} = 2n$ and $\chi_b^{(v)} = 2 - 2n$. In general, since the parts of the boundary used for closing the superclusters and the parts used for closing voids make the whole surface of the box

$$\chi_b^{(c)} + \chi_b^{(v)} = 2 \tag{30}$$

since the box surface is homeomorphous to a sphere and therefore is equal to two. Summing up the cluster ans void Euler characteristics one obtains

$$\chi^{(c)} + \chi^{(v)} = 2\chi^{(p)} + \chi_b^{(c)} + \chi_b^{(v)} = 2(\chi^{(p)} + 1). \tag{31}$$

Thus, the global Euler characteristic for periodic boundary conditions, $\chi^{(p)}$ can be found if both $\chi^{(c)}$ and $\chi^{(v)}$ are computed at the same threshold under assumption of non-periodic boundary conditions

$$\chi^{(p)} = \frac{1}{2}(\chi^{(c)} + \chi^{(v)}) - 1. \tag{32}$$

Computing $\chi^{(c)}$ and $\chi^{(v)}$ also assumes that all individual clusters and voids have closed surfaces. The surfaces of su-

perclusters and voids cut by the boundary of the box are closed by necessary parts of the box boundary surface.

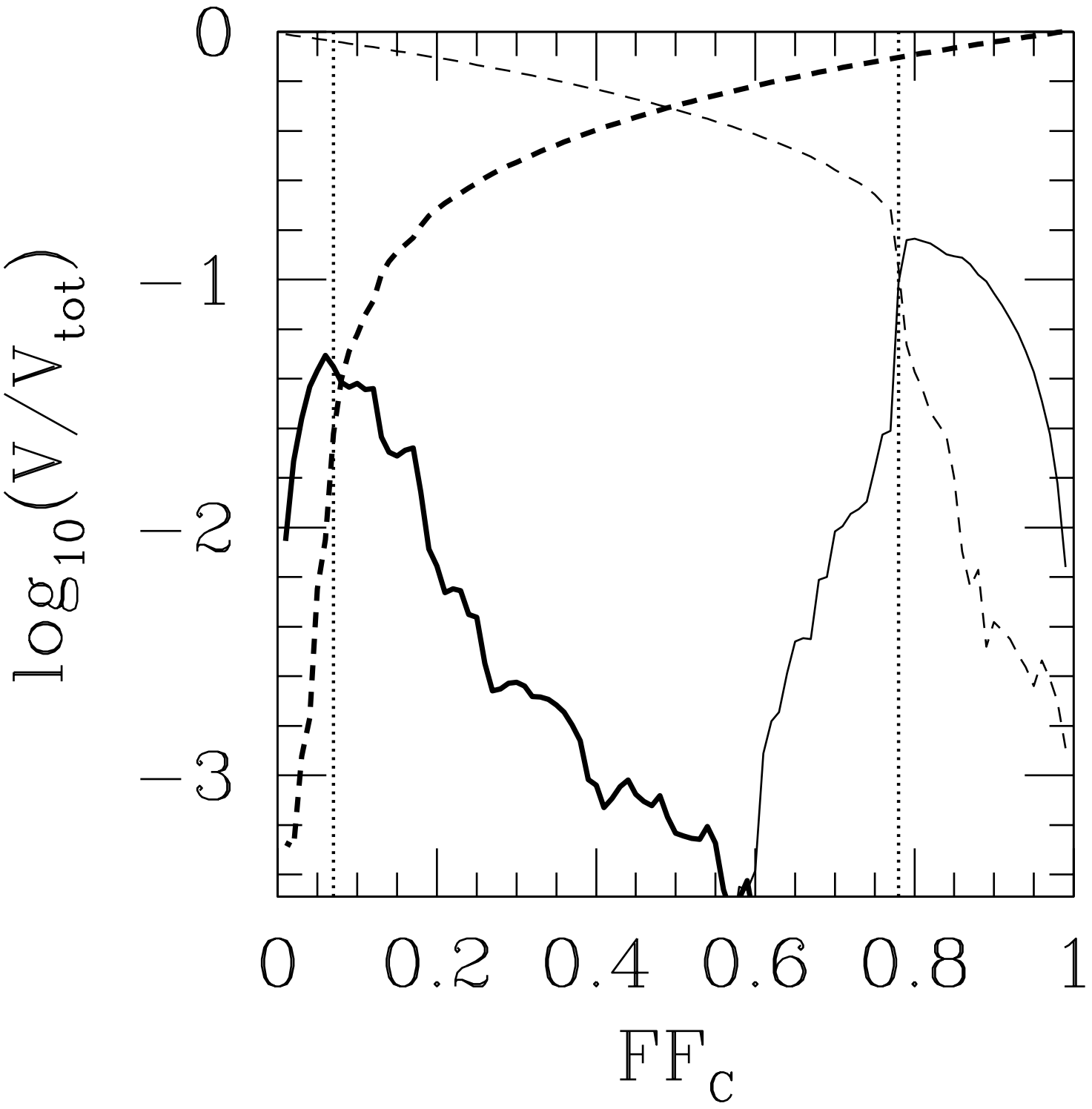
0
−1
−2
−3
$\log_{10}(V/V_{tot})$
0
0.2
0.4
0.6
0.8
1
FF_c